ORIENTAL JOURNAL OF CHEMISTRY
An International Open Access, Peer Reviewed Research Journal
www.orientjchem.org

ISSN: 0970-020 X
CODEN: OJCHEG
2024, Vol. 40, No.(6):
Pg. 1823-1835

Plant Mediated Synthesis Cu-Ag-Ru Trimetallic Nanoparticles Using *Andrographis paniculata* Extract: Antibacterial, Anticancer and Photocatalytic activities

RATHIKA RADHAKRISHNAN[1]* and S. SRINIVASAN[2]

[2]Department of Chemistry, Annamalai University, Annamalai Nagar, Chidambaram, Tamil Nadu, India.
[1]Department of Chemistry, Annamalai University. 9/34, Mariyamman Koil Street, Ceeyapadi, Bhuvanagiri, Cuddalore district, Tamil Nadu, India.
*Corresponding author E-mail: rathikaradha1997@gmail.com

http://dx.doi.org/10.13005/ojc/400635

(Received: May 25, 2024; Accepted: December 12, 2024)

ABSTRACT

In the current investigation, Cu/Ag/Ru trimetallic nanoparticles (TNPs) were produced using *Andrographis paniculata*, a medicinal herb known for its antibacterial, anticancer, antifungal, antiviral properties, and extensive therapeutic uses. Recently, nanotechnology has become essential for the progress of research and addressing environmental pollution issues. These trimetallic or polymetallic nanoparticles has been synthesized and characterized further. The presence of TNPs was confirmed through UV, FTIR, SEM, and EDX analyses. UV studies indicated that the TNPs exhibited absorption peaks within the range of 200 to 400 nm. The various phytochemical constituents such as alkaloids, terpenoids, aldehydes, ketones, and phenols present in the plant were identified by FTIR analysis. The size, morphology, elemental composition, crystallinity, and three-dimensional structure of the TNPs were verified using SEM, EDX, XRD, and AFM techniques. The dimensions of the TNPs ranged from 20 to 60 nm. The TNPs demonstrated remarkable results in both antibacterial and photocatalytic activities, particularly in dye degradation. The different bacterial strains were utilized effectively for anticancer studies. To reduce the use of harmful substances that can impact the environment, the TNPs were synthesized biologically, making them eco-friendly, cost-effective, and devoid of harmful byproducts in the synthesis process.

Keywords: Trimetallic nanoparticles, Crystallinity, Antibacterial, Anticancer, Antifungal, Antiviral, Photocatalytic activities, Eco-friendly, Cost-effective.

INTRODUCTION

Cancer ranks among the most lethal diseases, resulting in deaths prior to the age of 70 across the globe. According to GLOBOCAN, cancer cases are on the rise, leading to over 9.6 million fatalities worldwide, with predictions indicating further increases by 2040[1]. It appears that one in nine individuals is likely to develop cancer during their lifetime. High rates of lung cancer are observed in males, while breast cancer predominates in females. In children, cancers such as lymphoid leukemia affect boys (29.2%) and girls (24.2%). It was estimated that the incidence of cancer cases will rise from 1.46 million (2022) to 1.57 million(2025[2]. Factors such as rapid urbanization, an older demographic, sedentary and unhealthy lifestyles, fast-food consumption, and air pollution–both indoor and outdoor–seriously impact individuals in middle- to low-income countries like India[3].

The Indian Council of Medical Informatics and Research (NCDIR) and the National Cancer Registry Programme (NCRP) provide crucial statistics on cancer cases. The data indicates that cancer prevalence is higher among males than females[4]. Numerous synthetic medications are available, but they often come with side effects. Chemotherapy and radiation therapy have been developed as cancer treatment options, though they also carry side effects[5]. The discovery of drugs through biological methods has led to the identification of many treatments derived from various medicinal plants aimed at addressing diseases[6]. Drugs sourced from medicinal plants have shown effectiveness and minimal side effects[7].

Andrographis paniculata is a traditional Ayurvedic remedy, part of the Andrographis genus in the Acanthaceae family, which consists of 40 species. Commonly known as the King of Bitter (Kalmegh), it is an annual, branched herb utilized for various health issues[8]. The decoction of this plant is utilized for treating ailments such as fever, colic, the common cold, leucorrhea, prenatal and postnatal care, jaundice, gonorrhea, wounds, and snake bites[9,10]. This plant is used to treat respiratory infections, sore throats, and chronic diseases. It naturally possesses antimicrobial[11], anti-inflammatory[12], antioxidant[13], antiallergic and hepatoprotective activity, and nephroprotective activity[14]. It was found to have high efficacy in anticancer activity against neuroblastoma (IMR-32) and human cell lines[15]. Some of the compounds in *Andrographis paniculata*, such as 14-deoxyandrographolide and hydroandrographolide. These compounds, at higher concentrations, have highly effective cytotoxicity towards HPBL[16,17].

Nanomedicine involves the application of knowledge and tools of nanotechnology to diagnose, treat, and prevent disease with minimal side effects[18]. Nanomaterials are attractive due to their innovative methodologies and glorious applications because of their physical, chemical, biological, optical, and electrical properties. Some metals like palladium, silver, gold, ruthenium, and copper nanoparticles were synthesized by various routes, and the formation of nanoparticles depends upon the particle size and shapes[19].

Nanomaterials have a wide spectrum of applications in areas ranging from catalytics, photonics, molecular computing, energy storage, fuel cells, tuneable resonant devices, sensors, etc. This is because of increased reactivity in nanoscale materials when compared to their nanosized counterparts[20]. In fact, it has special properties such as small dimensions, electrical, mechanical, optical, magnetic, and thermal stabilizing properties, and a high surface-to-volume ratio. The surface coating of nanoparticles (NPs) also plays a significant role. Metallic NPs are catagorised into monometallic, dimetallic and polymetallic nanoparticles depending upon the number of metals and oxidation state of the metals. These polymetallic nanoparticles(NPS) have attracted attention because of their enhanced catalytic properties[20]. The bioengineered NPs are designed to remove harmful particles from the polluted water. Since it is toxic to heavy metals from industries and wastewater from households[21].

Multi-metallic NPs are generally considered novel materials because they incorporate two or more metals to make alloys. The Multi metallic NPs can be modified to enhance their physicochemical and morphological properties throuigh controlling its structure, temperature,kinetic factor, and shapes to achieve maximum potential and applications. It was concluded that the Multi metallic NPs have specific characteristics that result from the combined effects of individual metals[22]. The cytotoxicity of metallic NPs synthesized in an aqueous medium of plant extract depends upon the time, dose, etc., particularly their size and shape. It was reported that the smaller size of the NPs was more potent than other shapes. The metallic NPs were closely associated with the generation of reactive oxygen species (ROS). During the DPPH scavenging activity, the diluted NPs were suspended in an aqueous solution of 0.02% to assess the radical scavenging activity[23].

Nanoparticles as drug carrier

Several improvements have been made to chemotherapy over the past 25 years. Some drugs are proven to have excellent efficacy but cause severe side effects and also affect the quality of life. More importantly, these drugs are very expensive. For example, dEPoB was synthesized based on the mechanism of action of paclitaxel and reported to be more efficient than paclitaxel. The discovery of new drugs is a slow process to reduce the existing side effects. However, the ideal chemotherapeutics can be achieved, which requires a high level of concentration of drugs able to concentrate affected cells without disturbing non-targeted tissues and organs. They should be designed in such a way to cause very minimal or no side effects. This concept, also known as 'magic bullet', comes from the experience of German chemist Paul Ehrlich. The magic bullet consists of two components. One should be designed to recognize the target cells and bind to them. Another should play a therapeutic role in this target. In many cases, anticancer payloads, namely radionucleotides, toxins, and chemotherapeutic agents, have been delivered to tumors via monoclonal antibodies[24]. The various pharmaceutical carriers, including polymers, microcapsules, microparticles, cells, cell ghosts, lipoproteins, liposomes, and micelles, have been used as carriers to multiply the number of drug molecules per target without affecting the normal surrounding cells and tissues. There has been recent progress in the development of nanoparticles. The different kinds of nanoparticles, such as organic, inorganic, and hybrid nanoparticles, are designed to improve the interaction between the biomolecules, controlled transport, and releases[25].

Synthesis of Nanoparticles

The various physical and chemical methods, such as electrochemical, ultrasonication, chemical vapor deposition, etc., are significant; the formation of NPs depends upon the process, such as the kinetics of interaction between the metal ions with the reagent, adsorption, influence in morphology, and physiochemical parameters[26,27]. Fig. 1. shows the classification of nanoparticles based on the methods of synthesis.

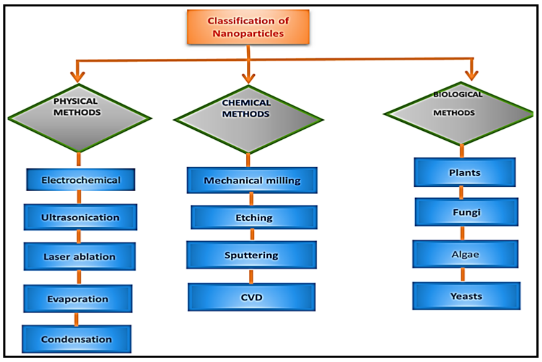

Fig. 1. Different methods of synthesis of nanoparticles

The metallic nanoparticles Ru, Ag, and Pd were produced from the aqueous extract of garlic tunicate leaves. The average dimensions of these TNPs ranged from 50 to 90 nm[28]. Copper oxide nanoparticles were synthesized using the leaf extract of the Ficus religiosa. Additionally, the anticancer properties can be evaluated at varying concentrations of CuO NPs, which were identified to be 200 µg/mL in A549 cells after 36 hours[29]. Silver nanoparticles were generated using Andrographis paniculata through an extracellular approach[30]. Likewise, silver nanoparticles have been produced utilizing numerous plant extracts, including Areca catechu, Maesa calophylla, Maesa laxiflora, Adinandra poilanei, and others. Notably, the six extracts exhibited greater 2,2-diphenyl-1-picryl hydroxyl radical scavenging activity and reducing potential compared to any other extracts. The Ag NPs displayed significant negative zeta potential values, with hydrodynamic sizes ranging from 12.5±1.0 nm to 21.3±4.9 nm. Furthermore, they demonstrated substantial cytotoxic effects on A549 and HeLa cells[31]. Certain metal nanoparticles, including cadmium oxide (CdO), neodymium oxide (Nd_2O_3), and nickel nanoparticles, were synthesized using extracts of Andrographis paniculata, and these nanoparticles showed effectiveness in anticancer research employing MCF-7 cells[32,33].

MATERIALS AND METHODS

Materials

Copper sulfate, silver nitrate, and ruthenium chloride were brought from the Sisco Chemical Laboratory with high purity.

Preparation of TNPS

Approximately 10 g of fresh Andrographis paniculata leaves were gathered, thoroughly rinsed with tap water to eliminate any contaminants, and then allowed to dry at room temperature. About 250 milliliters of double-distilled or deionized water was used. Around 150 milliliters of this water was added and boiled for one hour at 60°C to create a plant extract. The resulting solution took on a straw yellow hue. The solution was left overnight and then filtered using Whatman 40 filter paper.

Approximately 3 milliliters of 0.1 N copper sulfate, silver nitrate, and ruthenium chloride were incorporated and heated to 70°C for one hour. Subsequently, the precursor solution was combined with the extract solution, resulting in a color change from straw yellow to black. The solution was placed on a magnetic stirrer and left still at room temperature. The precipitate that formed was filtered, rinsed with ethanol several times to remove any impurities, and then dried in an oven at 150°C. Consequently, TNPs were produced and are available for characterization for further analysis and overall process were given in Figure 2.

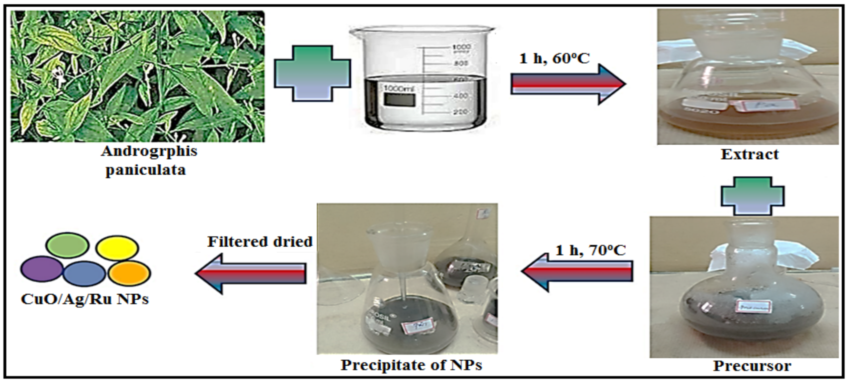

Fig. 2. Preparation of biosynthesized CuO/Ag/Ru TNPs via the leaves extract of *A. paniculata*

Characterization of TNPs

The biological preparation was initially validated through UV-Visible spectroscopy. It was subsequently analyzed using a SHIMADZU-UV 1800 UV-Visible spectrophotometer and quartz, utilizing a 10 mm path length. This device is employed to acquire qualitative information about substances via their characteristic absorption patterns present in the samples. The morphology of the nanoparticles (NPs) can be verified using scanning electron microscopy (SEM) and atomic force microscopy (AFM). The SEM (model: JEOL-JSM-IT200) operates at an accelerating voltage range of 0.5 kV to 30 kV, with images captured at various magnifications, including 1500X, 5000X, and 10,000X, among others. The interactions between metals and the biochemical compounds found in the NPs can be explored with Fourier-transform infrared spectroscopy (FTIR). The elemental makeup and ratio of individual metals within the TNPs can be assessed using energy dispersive X-ray spectroscopy (EDX). Additionally, the crystallinity and average size of the NPs can be gauged through X-ray diffraction (XRD). X-ray photoelectron spectroscopy (XPS) (model: K alpha) can be employed to validate the formation of NPs and the oxidation states of the metals in the materials. The decomposition, melting points, purity, and energy transitions may be examined with a thermal analyzer (model: NETZSCH-STA449F3 Jupiter). The temperature can be varied from room temperature up to 1400°C at a rate of 10,200°C/min in a volume of 10 mL liquid within a blank atmosphere. TEM and DLS are used to assess the morphological aspects of trimetallic nanoparticles.

RESULT AND DISCUSSION

UV-Visible

The UV-Visible spectroscopy used to assess the formation of nanoparticles and the absorption of the biological TNPs was measured in the range of 200–400 nm. The strong surface plasmon peaks observed at 210nm and 330nm correspond to metals such as CuO, Ag, and Ru NPs. These resonance peaks confirm the formation of the inner and outer cores of TNPs. Moreover, the formation of NPs can be visually confirmed by the color changes from straw yellow to black, and Figure 4.1. represents the UV-visible spectra of TNPs.

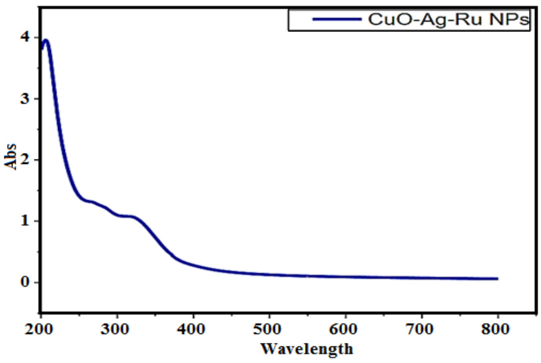

Fig. 4.1. UV-Visible spectra of CuO/Ag/ Ru TNPs

FTIR

Different functional groups, including ketones, aldehydes, alkaloids, and terpenoids, in the plant extract contribute to the reduction of metals into metallic nanoparticles (NPs). This research aimed to identify the functional groups present in the NPs, as well as to assess the interaction between the metal and the plant extract. The observed bands at 3360, 2900, 1720, and 1160 cm^{-1} correspond to the stretching vibrations of OH, C-H, C=O, C=C, and C-O, respectively. The functional groups found in the TNPs suggest the presence of bioorganic compounds such as phenols, amino acids, and carboxylic acids, among others[33,34]. A band detected at 3390 and 1640 cm^{-1} is associated with C=O stretching vibrations from carboxyl groups and C=N bending from amide groups. The band around 1590 cm^{-1} aligns with the N-H band of primary amines found in the Andrographis paniculata extract. The approximately 2900 cm^{-1} band corresponds to phenolic and alcoholic compounds in the Andrographis paniculata extract. The slight overlapping bands in this spectrum indicate that the extract of Andrographis paniculata is integrated with the metal NPs. Additionally, the bands observed below 600 cm^{-1} are primarily attributed to the metal-metal interactions within the TNPs[33].

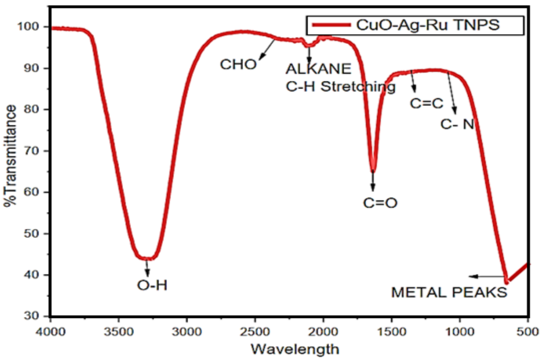

Fig. 4.2. FTIR spectra of CuO/Ag/Ru TNPs

SEM AND EDX

The dimensions and configuration of the TNPs can be assessed through SEM analysis, Fig. 4.3 illustrates the SEM analysis at various magnification levels of 1 m, 5 m, 10 m, and 500 m, showing that the shape of the TNPs is spherical, manifesting an agglomerated structure where individual NPs cluster together. while EDX provides insights into the elemental composition of each TNP, as depicted in Fig. 4.3.1. In the EDX analysis, the metal NPs are composed of carbon (38.9%), oxygen (43.38%), copper (3.2%), ruthenium (4.7%), and silver (10.21%), respectively.

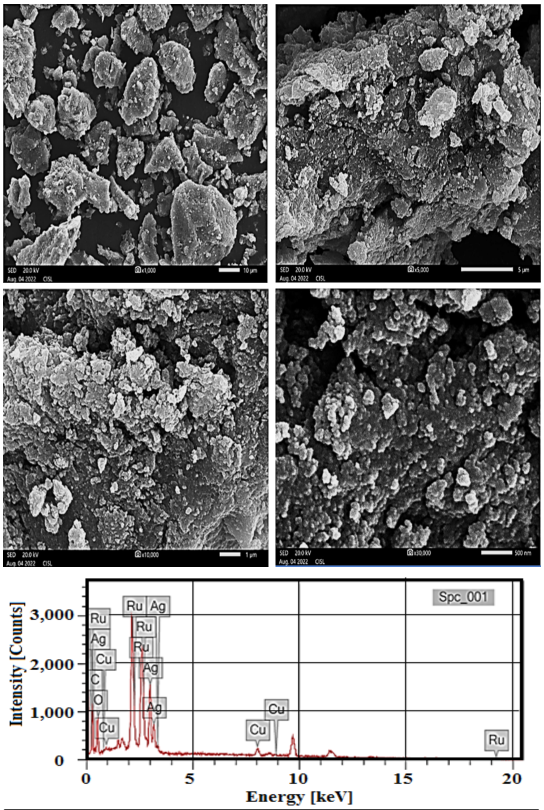

Element	Line	Mass%	Atom%
C	K	15.72±0.12	38.47±0.30
O	K	23.62±0.41	43.38±0.75
Cu	K	6.98±0.24	3.23±0.11
Ru	L	16.21±0.31	4.71±0.09
Ag	L	37.46±0.37	10.21±0.10
Total		100.00	100.00

Fig. 4.3 shows SEM analysis of TNPs at 10 μm, 5 μm, 1 μm and 500 μm respectively and Fig 4.3.1. shows EDX spectra of TNPs

XRD

The material's lattice, crystallinity, average size, and crystal orientation of the NPs can be investigated using XRD analysis. The observed diffraction sharp peaks positions at 2θ = 32.590, 35. 610, 38.780, 48.820, 53.37, 66.31, 68.15, 72.4 were assigned to (110), (-111), (111), (-202), (020), (202), (-113), (-311), (220), (-220), and (311) are consistent with the previous literature (JCPDS No. 01-080-0076) of copper oxide NPs with a monoclinic phase[34]. The prominent diffraction peaks at 2θ = 37.99, 46.29, 64.34, and 77.19 correspond to cubic crystalline Ag NPs with JCPDS No. 04-0783[35]. The diffraction peaks of RU NPs were assigned to hexagonal the average size of the TNPs can be calculated by means of the Debye Scherrer formula, $D = K\lambda/\cos\theta$ where k is the Scherrer constant, λ = 1.5418A, β = 0.06, and $\cos\theta$ = 0.96[36]. In this formula, (0.90 x 1.5418)/(0.06 x 0.97) = 22.2nm. Thus, the diameter of the crystallite is about 22nm.

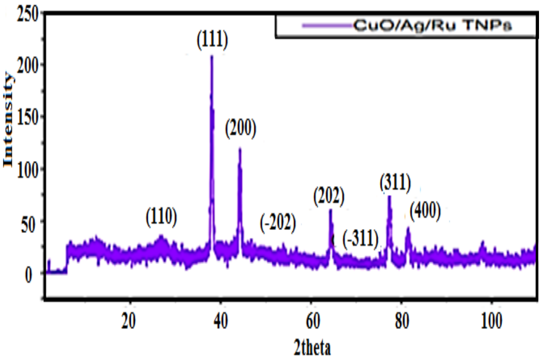

Fig. 4.4. XRD spectra of CuO/Ag/Ru TNPs

TEM & DLS

From the TEM analysis, it was observed that CuO/Ag/Ru trimetallic nanoparticles composed of spherical, flake, and cup-shaped morphology and the size of the nanoparticles was 25-100 nm (Fig. 4. 5) and in good agreement with the DLS, XRD, and AFM values. The agglomerated form of the nanoparticles was similar to the SEM morphology. Further, these morphologies were compared with the reported previous literature of individual metal nanoparticles. DLS spectra also observed that the maximum intensity was between 1-100 nm with a diameter of 192.5 nm and a standard deviation of 176. Dynamic Light Scattering (DLS) analysis was performed using a Micromeritics instrument, specifically the Nanoplus model. This equipment is capable of measuring the particle sizes of liquid-suspended samples through a dilution method, covering a size range from 0.1 nm to 12.3 µm, with sample concentrations varying from 0.00001% to 40% and a sensitivity for molecular weights as low as 250 Da. DLS provides insights into the dimensions of the nanoparticles produced. Dynamic light scattering illustrates the behavior of nanoparticles as well as their tendency for agglomeration or settling. A light source is introduced into the cell, and the scattered light is captured and analyzed to determine the particle size. The particle size is recorded at an average diameter of 192.5 nm, with a standard deviation of 176 and a refractive index of 1.3 as shown in Figure 4. 5.1.

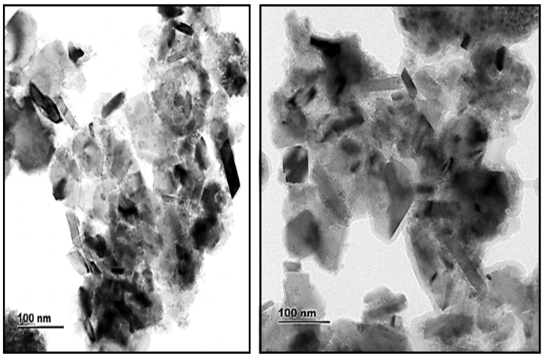

Fig. 4. 5. TEM images of CuO/Ag/Ru TNPS

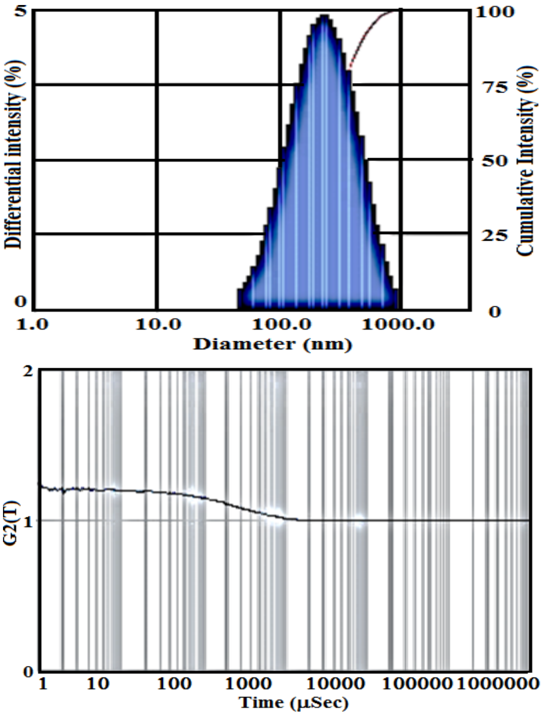

Fig. 4. 5. 1. DLS spectra of CuO/Ag/Ru TNPs

AFM

It is an advanced technique to assess the size, shape, and dispersion of TNPs. Here, the sample is dissolved in a suitable solvent and dried as a thin layer on a mica-based glass slide[37]. Fig. 4.6. shows two-dimensional, three-dimensional, and particle-size histograms of TNPs. From the SEM and AFM studies, it was confirmed that the TNPs are spherical-shaped and agglomerated, with an average particle size of about 22 nm.

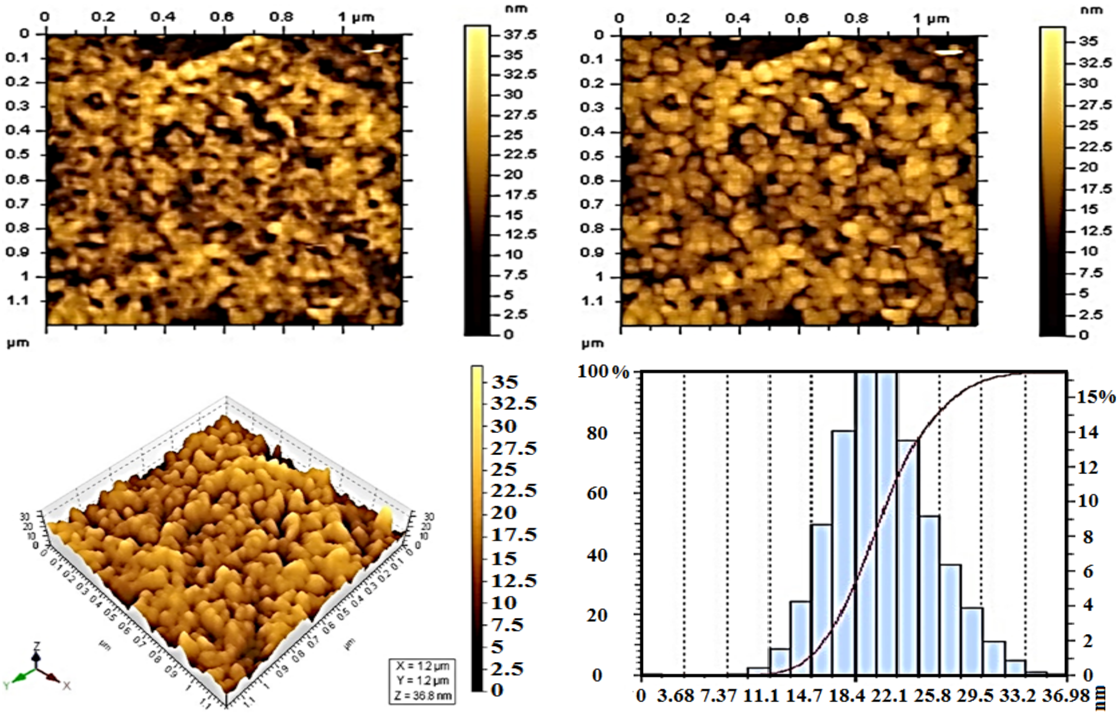

Fig. 4. 6. AFM spectra of CuO/Ag/ Ru TNPS

XPS

XPS is used to determine the conformation and oxidation states of metals in TNPs. The binding energy of elements sch as O,Cu, Ag, Ru are given in the Table 1. The binding energy of Ru(3d) is 285ev, O(1s) is 532ev, Ag(3d) is 368ev, and Cu(2p) is 935ev. The XPS spectra of individual elements are given in Fig. 4.7. The XPS survey spectra the Ag existed as Ag(3d) and Ag(3p3) with the binding energies 368ev and 560ev respectively separated by 200ev.

Table 1: XPS spectra of CuO/Ag/Ru TNPs

Name	Peak BE	FWHM eV	Area (P) CPS.eV	Atomic %
Ru 3d	285.9	2.4	104601.28	1.32
O 1s	532.45	4.18	1232073.04	95.44
Cu2p	935.26	2.22	256830.11	3.23
Ag3d	368.3	2.59	268564.2	1.7

Thermal analysis (DTA/TGA)

DTA/TGA is utilized to evaluate the thermal properties of the sample, which include decomposition, melting point, glass transition, oxidation rate, crystallinity degree, purity, transition energy, etc. A sample of 50–100 mg of CuO/Ag/Ru TNPs was placed in an Al_2O_3 crucible, and the temperature was maintained between 20 and 700°C. As the temperature rises, the material begins to decompose at approximately 250°C, with the reaction being exothermic and the stable metal nanoparticles remains above 600^{0}C, as shown in Figure 4. 8.

Photocatalytic activity of TNPs

The photocatalytic activity of TNPs can be performed using methylene blue dye in a UV-irradiated photoreactor, and this methylene blue (MB) shows characteristic absorption peaks from 200 to 400nm. The decolorization process occurs when UV light is irradiated on the solution to the concentration of X10^{-3} M at various concentrations. The effectiveness of degradation process on the nature of the substance used, time, and the binding of catalyst with the molecules of MB dye that have degraded. This increases the active sites of the photocatalyst surface and free hydroxyl radicals. During this process, the dark blue of the dye diminishes over time because the TNPs act as scavengers that are applied to the active sites of the photocatalyst. Importantly,the formation of reactive oxygen species (ROS) results from the electron-hole pair surface transmission process. These generated ROS are responsible for the photocatalytic activity of TNPs[38].

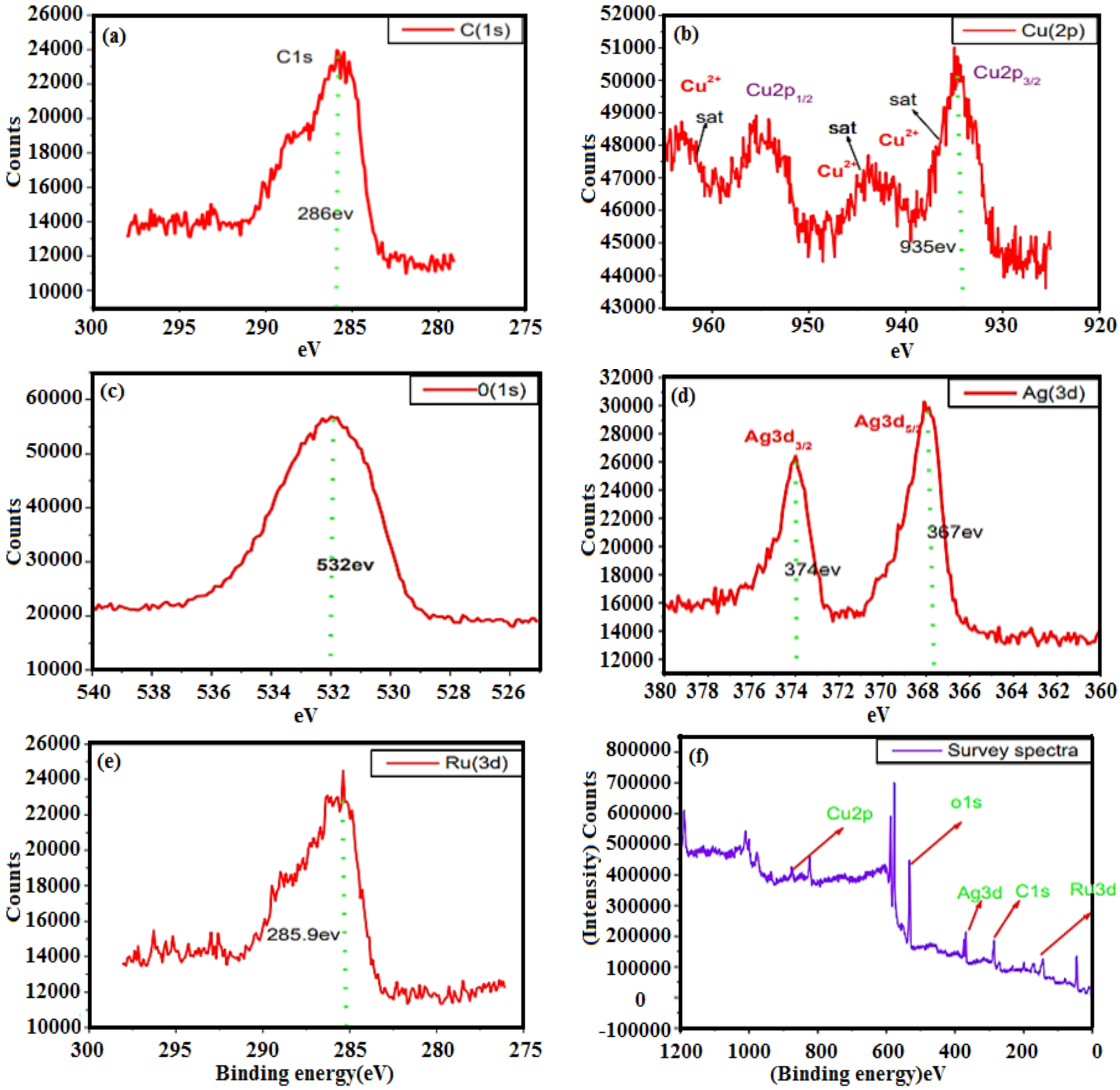

Fig. 4. 7. XPS spectra of Cu(2p), O(1s), Ag(3d), C(1s), Ru(3d) and XPS survey spectra of CuO/Ag/Ru TNPs

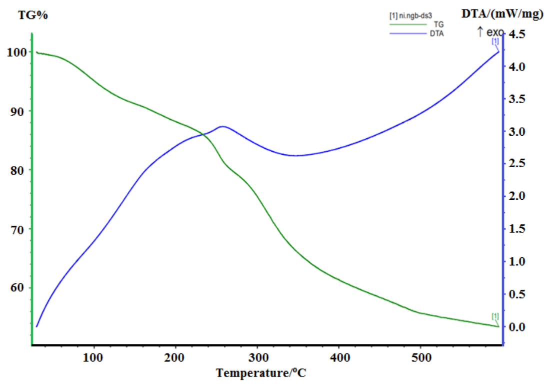

Fig. 4.8. Thermal studies (DTA/TG) of CuO/Ag/Ru TNPs

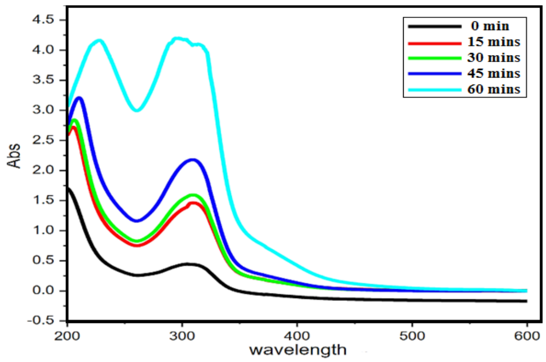

Fig. 5. Photocatalytic activity of CuO/Ag/Ru TNPs using Victoria blue dye

Antibacterial activity of TNPs

The microbial strains of *Escherichia coli, Streptococcus pyogenes, Staphylococcus aureus*, and *Klebsiella pneumonia* used to examine the antibacterial activity of the TNPs at different concentrations are shown in Table 2, and the image were given in Fig. 6.2. The zone of inhibition values for TNPs against bacterials strains at three different concentrations (25 µl, 50 µl & 50 µl) are graphically represented in the Fig. 6.1. The mechanism behind the antimicrobial activity is that the higher biological content of the TNPs, indicated by potential disruption of the membrane, damage to DNA, and production of reactive oxygen species such as peroxide, superoxide, inactive species, etc., can eliminate or reduce bacterial growth and, intricately with the membrane, lipids, and enzymes, induce cellular death. The hybrid TNPs exhibited higher antimicrobial activity than the individual metal NPs[28].

Table 2: Antibacterial activity of CuO/Ag/Ru TNPs using different pathogens at various concentrations & Fig. 6.1. The graph of maximum antibacterial activity of Cu/Ag/Ru TNPs against *E. coli, S. pyogenes, S. aureus*, and *K. pneumonia*

Test bacterial pathogens	Zone of inhibition (mm) 25 mg	52 mg	75 mg	Chloramphenicol (5 mg)
S. aureus	10±0.51	13±0.29	17±0.34	32±1.09
S. pyogens	14±0.52	17±0.30	17±0.39	31±1.09
K. pneumonia	19±0.51	138±0.26	16±0.35	29±1.09
E. coli	11±0.52	12±0.28	14±0.30	31+1.09

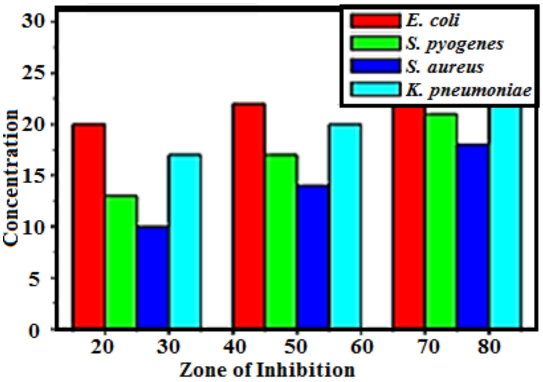

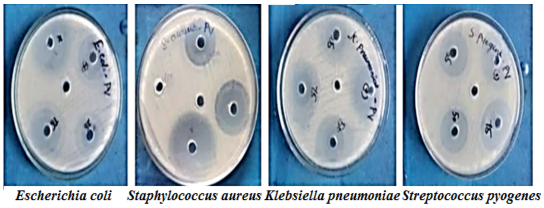

Fig. 6.1. Antibacterial activity of CuO/Ag/Ru TNPs using strains of *E. coli, S. pyogenes, S. aureus,* and *K. pneumonia*

Anticancer activity

The yellow compound 3-4,5-dimethylthiozol-2-Yl-2,5-diphenyltetrazoliumbromide (MTT) is transformed by mitochondrial dehydrogenase in healthy cells, producing a quantifiable purple product. Living cells possess NAD(P) H-dependent reductase, which converts the MTT reagent into formazan, resulting in a deep purple color. The crystals of Formazan crystals are dissolved with the solubilizing solution, and the absorbance are usually recorded between 500 and 600 nm by a plate reader. A total content was dissolved in a 50 mg of MTT with approximately 10 mL of PBS. After vortexing for one minute, it was filtered through 0.45-micron filters. The flask was wrapped in aluminum foil to protect it from light, given that MTT is sensitive to light. This solution was stored about 4°C for further incvestigations.

For the cell viability assessment, TNPs-1 viable cells were collected and counted with a hemacytometer, then diluted in DMEM medium to achieve a cell density of 1 × 10^4 cells/mL. They were placed in 96-well plates, with one well per cell, and incubated for 24 h to facilitate attachment. Subsequently, TNPs-1 cells were treated with a control and various concentrations (10–70 µg/mL) of aqueous extracts were administered to each well. The cells were subjected to inubation at 37°C in a wet condition where it containing 95% air and 5% CO_2 for 24 hours. Following the incubation period, the drug-treated cells were thoroughly washed with fresh culture medium, and MTT (5 mg/mL in PBS) dye was added to each well. This content was subjected incubation for 4 h at 37°C.

The purple precipitate of formazan that formed was dissolved in 100 µL of concentrated DMSO, and cell viability was assessed by measuring absorbance at 540 nm using a multi-well plate reader. The results were expressed in terms of percentage of values viable cells compared to the control values. The half-maximum inhibitory concentration (IC_{50}) values were determined, and the optimal doses were evaluated at various time points[39,40]. The IC_{50} values were derived from the dose-response curve of the aqueous extract, where a 50% reduction in cytotoxicity was compared to that of control cells. All experiments were conducted at least three times, with three replicates each. The MTT assay results at varying concentrations are presented in Table 3, and the graphical representation of the MTT assay for CuO/Ag/Ru TNPs tested against MCF-7 cells is illustrated in

Fig. 7. The images of both the treated and control groups from the MTT assay for CuO/Ag/Ru TNPs against MCF-7 cells are displayed in Figure 7.1.

Inhibitory of cell proliferation %

$$= \frac{\text{Mean absorbence of the control- Mean absorbence of the sample X 10}}{\text{Mean absorbence of the control}}$$

Statistical analysis

The statistical comparisons were performed by one-way analysis of variance (ANOVA), followed by Duncan's multiple range test (DMRT), using SPSS version 12.0 for Windows (SPSS Inc., Chicago; http://www.spss.com). The values are considered statistically significant if the p value is less than 0.05[41,42].

Table 3: MTT assay of CuO/Ag/Ru TNPs at different concentrations

Ni	Blank	0	100	200	300	400	500	600	700	800	900	1000
A	0.06	1.38	1.53	1.48	1.27	1.02	0.83	0.60	0.68	0.53	0.52	0.48
B	0.06	1.67	1.47	1.20	1.26	1.24	0.97	0.82	0.82	0.76	0.75	0.52
C	0.03	1.75	1.43	1.18	1.13	1.09	1.02	1.20	0.73	0.65	0.54	0.45
Average		1.60	1.480	1.291	1.221	1.123	0.947	0.881	0.748	0.68	0.607	0.485
% of Inhibition		0	8	19	24	30	41	45	53	57	53	70

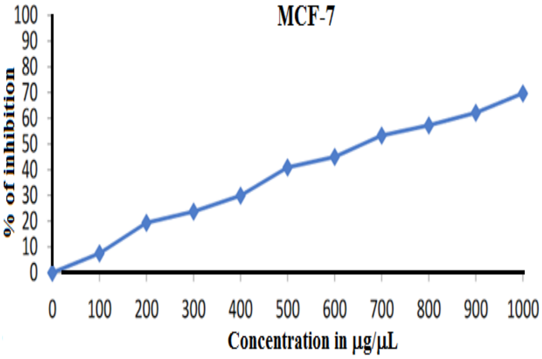

Fig. 7. Graphical representation of MTT assay of CuO/Ag/Ru TNPs against MCF-7cells

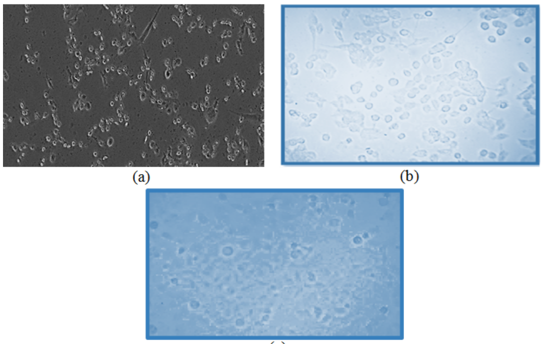

Fig. 7.1. The images of treated and controlled MCF-7 breast cancer cells using CuO/Ag/Ru TNPs

Antioxidant activities

DPPH (free radical scavenging activity), the DPPH molecules has stable nitrogen radicals used to study the free radical quenching activity of different antioxidants. The DPPH assay was performed with the reference substance ascorbic acid acts as positive control. The TNPs were dissolved with suitable solvent like deionised water at different concentrations as shown in Table 4.

The antioxidant activity of TNPs increases with increasing concentrations. The measurement was performed at five different concentrations and plotted to calculate R^2 value as shown in Fig 8 & 9. The antioxidant activity is the ability to protect from oxidative damages and IC_{50} values were found to be 107.8 µg/mL and R^2 value is 0.912. Furthermore, this result is good agreement with the antioxidant activity values of individual nanoparticles. The percentage of radical scavenging activity (%) can be calculated using the following equations.

$$\text{Radical scavenging activity (\%)} = \frac{OD_{control} - OD_{sample}}{OD_{control}} \text{ X 100}$$

Table 4: Antioxidant activity of TNPs at different concentrations & Fig. 8. Graph of antioxidant activity of TNPS with positive control

Test	Concentration of sample (mg/mL)	% of Inhibition of Nanoparticles	Ascorbic acid
	50	31.3	40
	100	39.2	50
IC_{50} Value	150	48.8	60
	200	59.2	70
	250	68.6	80
	108.8	150	

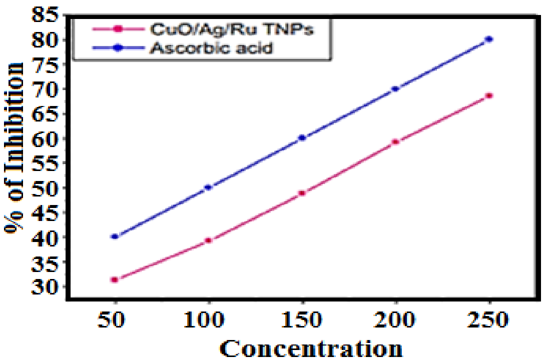

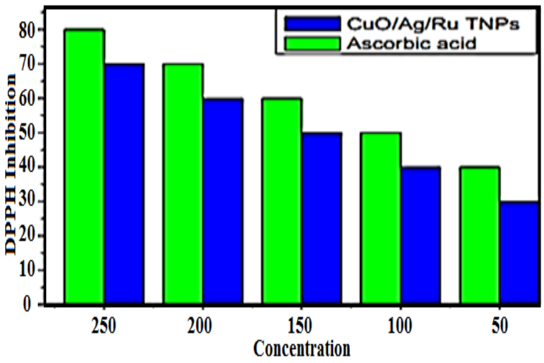

Fig. 9. Graphical representation of antioxidant activity of CuO/Ag/Ru TNPs at different concentrations

CONCLUSION

This green method provide great opportunities to develop more complex nanomaterials with good yield with less minimal of reactants. The trimetallic nanoparticles are usually greater performance in properties with enourmous applications and outcomes. This nanoparticles shows highly selective in catalytic action in photocatalytic activities. It has unique antibacterial activity against bacterial strains. It exhibit superior anticancer activities against human breast cancer cells even in minimum concentrations. This nanoparticles has distinct shape can help bind with the active site of the drug molecules. It can be used as potential drug carrier with minimum harmness to the normal cells.

ACKNOWLEDGMENT

I thanful to my Research supervisor, Dr. S. Srinivasan, Associate Professor, Annamalai University.

Conflict of interest

The author declare that we have no conflict of interest.

REFERENCES

1. Bray F.; Ferley J.; Soarjomataram I.; Siegel LR.; Torre AL.; Jemal A“ Global cancer statistics 2018 : GLOBOCAN estimates of incidence and mortality worldwide for 36 cancers in 185 countries”., *CA Cancer J. Clin.*, **2018**, *68*, 394-424.
2. Krishnan Sathishkumar.; Meesha Chaturvedi.; Priyanka Das.; S.Stephen and Prashant Mathur, “Cancer incidence estimates for 2022 & projection for 2025; Result from National cancer registry programme India”., *Indian J Med Res.*, **2022**, *156*, 598-607.
3. Vaitheeswaran Kulothungan.; Krishnan Sathishkumar.; Sravya Leburu.; Thilagavathi Ramamoorthy.; Santhappan Stephen.; Dharmapa Basavajappa.; Nifty Tomy.; Rohith Mohan.; Geetha R. Menon, and Prashant Mathur “Burden of cancers in India– estimates of cancer crude incidence, YLLS, YLDS and DALYs for 2021 and 2025 based on National cancer registry program., **2022**, *22*, 527.
4. Cherian Varghese “ Cancer prevention and control in India“
5. Hogland HC, Haemotological complications of cancer chemotherapy., *Semki Oncol.*, **1982**, *9*, 95-102.
6. Joselin J.; Jeeva S.; Andrographis paniculata : A review of its traditional uses, phytochemistry and pharmacology., *Med Aromat plants.,* **2001***, 3*, 169.
7. Fransworth NR: Screening plants for new medicines, Chapter 9, edited by Wilson E, Washington D.C, National Academy press; **1988**.
8. Perry L M, Medicinal plants of East and South east Asia : attributed properties and uses. Cambridge : MIT Press., **1980**.
9. Agbonlahor Okhuarolea.; Joyco Ehrizoghi Faloda Osayemwenre Erharuyi.; Vincent Imieji.; Abiodun Falodun.; Peter Langer.; Harnessing the medicinal properties of Andrographis paniculata for disease and beyond : a review of its phytochemistry and pharmacology., *Asian Pae J Trop Dis.*, **2014**; *4*(3), 213-222.
10. Zaiden. MR.; Noor.; Rain A.; Badrul. AR.; Adlin A.; Norazah. A, and Zakiah.I, In vitro screening of five local medicinal plants for antibacterial activity using disc diffusion method., *Trop Biomed.*, **2005**, *22*, 165-170.
11. Abu–Ghefreh,. AA.; Canatan. H, and Ezeamuzie CI, *In vivo* and *in vitro* anti-inflammatory effects of Andrographolide., *Int Immunopharmacol.*, **2009**, *9*, 313-318.
12. Trinedi NP and Rawal.UM, H, Hepatoprotective and antioxidant properties of Andrographis paniculata (Nees) in BHC-induced liver damage in mice., *Indian J Exp Biol.*, **2001**, *39*, 41-46.

13. Vetriselvan. S.; Rajamanickam. V.; Muthappan M, and Gnanasekaran D., Hepatoprotective effects of aqueous extract of Andrographics paniculata against CCl_4 induced hepatotoxicity in allerno wistar rats., *Asian Journal of Pharmaceutical and clinical Research*., **2011**, *4*(3), 93-94.
14. Rajeshkumar Shanmugam.; Mohammedi brahim Ponnanikajamideen.; M. Nagalingam.; Mahendran Vanaja., Anticancer activity of Andrographis paniculata leaves extract against microblastime (IMF-32) and human colon (HT-29) cancer cell line , world journal of pharmacy and pharmaceutical sciences, **2005**.
15. Ajaya Kumar, K. Sridevi, N.Vijaya Kumar, S.Nanduri, S. Rajagopal, Anticancer and immunostimulatory compounds from Andrographis paniculata., *Journal of of ethnopharmacology.,* **2004**, *92,* 291-295.
16. MM. Rahman.; F. Islam.; S.Afsana Mim., Multifunctional therapeutic approach of nanomedicines against inflammation in cancer and ageing., *Journal of nanomaterials*., **2022**, *2022*, Article ID 4217529, 19 pages.
17. A.M. Abu-Dief.; L.H.Abdel Rahman. MA.; Abd-El Sayed.; MM. Zikry and A.Nafady,Green synthesis of Ag nanoparticles utilizing Delonix Regia extract as anticancer antimicrobial agents., *Chemistry select.,* **2021**, 13263-13266.
18. C.N.Rao.; H.S.S.Ramakrishna Matte.; Rakesh Yoggu and A.Govindaraj.; Recent progress in the synthesis of inorganic nanoparticles., *Dalton Trans*., **2012**, *41*, 5089.
19. Sharma G.; Kumar.A.; Sharma. S.; Nushand.M, Prakash Dwaivedi. R Alothman, Z.A.; Mola, G.T.; Novel development of nanoparticles to bimetallic nanoparticles and their composites : *A review J. King Savd Univ. Sci*., **2019**, *31*, 259-269.
20. Sana Abbas.; Saima Nasreen.; Adeela Haron.; Muhammad Aqeel Ashraf.; Synthesis of Silver and Copper Nanoparticles from plants and applications as Adsorbents for Naphthalene decontamination., *Saudi Journal of Biological Sciences*., **2020**, *27*, 1016-1023.
21. Nagaraj Basavagowda and Kwang-Hyun Baek, *Multimetallic nanoparticles as Alternative Antimicrobial agents; challenges and perspectives molecules*., **2021**, *26*, 912,
22. Eun-Young Ahn.; Younie Park.; Anticancer prospects of silver nanoparticles green-synthesized by plant extracts., *Material science and Engineering* C116., **2020**, *111*, 253.
23. Kohler G and Milstein C: Continuous cultures of fuel cells secreting antibody of predefined specificity., *Nature.,* **1975,** *75*, 381-394.
24. Langer R: Drug delivery and targeting., *Nature.,* **1998***, 392*, 5-10.
25. Jin Zhang.; Christopher Q. Lens.; Michael Post.; Benott Simard.; Yues Deslandes, and Tsung Han Hsieh , Design of Nanoparticles as drug carriers for cancer therapy., *Cancer Genomics & Proteomics.,* **2006***,* 147-158.
26. D.R.Bhumkar.; H.M.Joshi.; Sastry,V.B.; Pokharkar, chitosan seduced gold nanoparticles as novel carriers for transmucosal delivery of insulin., *Pharm. Res*., **2007**, *24*(8), 1415-1426.
27. Prasad Govindrao Jamkharde.; Namerata W. Ghule.; Abdul Haque Baner.; Mohan G. Kalaskar.; Metal nanoparticle synthesis.; An overview on methods of preparation, advantage and disadvantages and applications., *Journal of Drug Delivery Science and Technology.,* **2019**, *53*, 101174.
28. Shaimaa Hussein.; Ayman M. Mahmond.; Hassan A. Elegebaly.; Omnia Magdyn Hendawy.; Emad H.M.Hassaneim.; Shaima M.N. Moustafa.; Nasssar F. Alotaibi, and Amr M.Nassar., *Journal of Chemistry*, **2022**, *14*, 3.
29. Renu Sankar.; Ramasamy Maheswari.; Selvaraju Karthik.; Kanchi Subramanian Shivashangari.; Vilwanathan Ravikumar.; Anticancer activity of Ficus religiosa engineered copper oxide nanoparticles., *Materials science and Engineering.,* **2014,** *44*, 234-239.
30. C. Pannerselvam.; S. Ponarulselvam and K.Murugan.; Potential Anti-plasmodial Activity of Synthesized Silver Nanoparticles using Andrographics paniculata Nees (Acanthaceae)., *Archives of Applied Science Research*., **2011**, *3*(6), 208-217.
31. M.Sundrarajan.; V. Muthulakshmi.; Green synthesis of ionic liquid mediated Neodymium oxide nanoparticles by Andrographis paniculata leaves extract for effective biomedical applications. S7213-3437(20)31065-4.
32. K. Karthik.; S. Dhanuskodi.; C. Gobinath.; S. Prabukumar.; S. Sivaramakrishnan.; Andrographis paniculata extract mediated green synthesis of CdO nanoparticles and its electrochemical and antibacterial studies., *J. Mater Sci:Mater Electron*., **2017**, *28*, 7991-8001.

33. Zahra Vaseghi.; Omid Tavakoli.; Ali Nematollahzadeh.; Rapid biosynthesis of novel Cu/Cr/Ni trimetallic oxide nanoparticles with antimicrobial activity., **2018**, 1898-1911.
34. Hojat Veisi.; Bikash Karmakar.; Taiebeh Tamoradi.; Rerza Tayebee.; Sami Jadifar.; Shahram Lotfi.; Behrooz Maleki & Saba Hemmati, Bio-inspired synthesis of palladium nanoparticles fabricated magnetic Fe_3O_4 nanocomposite over Fritillaria imperialis flower extract as an efficient recyclable catalyst for the reduction of nitroarenes, Scientific reports., **2020**, 4515.
35. Awadesh Kumar Mishra.; Kavindra Nath Tiwari.; Rajesh Saini.; Pradeep Kumar.; Sunil Kumar Mishra.; Virendra Bahadur Yadav.; Gopath Nath., *Journal of inorganic and organomateallic polymers and materials.,* **2020**, *30*, 2266-2278.
36. Haritha Meruvu.; Meena Vangalapati.; Seema Chaitanya Chippada and Srinivasa Rao Bammidi, Synthesis and characterization of Zinc oxide nanoparticles and its antimicrobial acti vity against *Bacillus substilis* and *Escherichia coli., Rasayan J.Chem*., **2017,** *4*(1), 217-222.
37. Ram Prasad and Vyshnava Satyanarayana Swamy, Antibacterial activity of Silver Nanoparticles Synthesized by Bark Extract of Syguim cumini., *J. Nanoparticles*., **2013**, 6.
38. Absulmohsen Ali Alsehri and Maqsood Ahmad Malik, Facile one pot Biogenic synthesis of Cu-Co-Ni Trimetallic Nanoparticles for enhanced photocatalytic Dye Degradation , **2020**.
39. J. Jayachitra.; M. Akshaya.; N. Pushpa.; R. Suja Pandian and C. Ruth Christiya,Anticancer activity, UV-Visible and FTIR analysis of Herbal formulation. Annals of R.S.C.B, ISSN: 1583-6258., **2021**, *25*(6), 5636-5655.
40. Tim Mosmann.; Rapid Colorimetric Assay for Cellular Growth and Survival ; Application to Proliferation and Cytotoxicity Assays., *Journal of immunological Methods*., **1983,** *65*, 55-63.
41. Yinmom Htun.; Shinji Nakamura.; Yasuhiro Nakao.; Tsutomu Mitsuie.; Kenichi Ohta.; Makota Arioka.; Takayuki Yokota.; Eri Inove.; Toi Tsuchiya Kosuke Koyano.; Yukihiko Konishi.; Takanori Miki.; Masaki Veno and Takashi Kusaka, Conflicting findings on the effectiveness of hydrogen therapy for ameliorating vascular leakage in a 5-day hypoxic-isochemic survival piglet model , Scientific report., **2023**, *13*, 10486.
42. Peter Larsson.; Hama Engquist.; Jana Biermann.; Elisabeth Werener Ronnerman.; Eva Forssell-Aronsson.; Amiko Kovaes.; Per Karlson.; Khalil Helon, and Toshima Z.Parris, Optimization of cell viability assays to improve replicability and reproducibility of cancer drugs sensitivity screens., Scientific reports., **2020**, 5798.